RMetS
Royal Meteorological Society

Effects of the changing heating profile associated with melting layers in a climate model

Hongyan Zhu,[a*] Eric Maloney,[b] Harry Hendon[a] and Rachel Stratton[c]
[a]*Science to Services, Bureau of Meteorology, Melbourne, Australia*
[b]*Department of Atmospheric Science, Colorado State University, Fort Collins, CO, USA*
[c]*Met Office, Exeter, UK*

*Correspondence to: H. Zhu, Bureau of Meteorology, GPO Box 1289, Melbourne, VIC 3001, Australia. E-mail: h.zhu@bom.gov.au

The impact of modifying the melting behaviour at the freezing level in the GA2.0 version of the Met Office Unified Model is investigated. By allowing snow to melt over a greater depth, biases in rainfall over the Maritime Continent (MC) are found to be improved, and there is an indication of benefits to the simulation of the Madden–Julian Oscillation.

Moistening diagnostics under weak temperature gradient theory are used to explain how and why changes to the treatment of melting influence tropical rainfall biases. The modified melting experiment increases the lower tropospheric diabatic heating rate per unit column-integrated convective heating in the MC, which helps to increase lower tropospheric vertical moisture advection per unit column convective heating, making conditions more favourable for convection there. Changes of the opposite sense occur in tropical ocean regions of the west Pacific and Indian Ocean. Changes in lower tropospheric radiative heating per unit convection produced by the different treatment of melting are particularly influential in engendering mean precipitation changes between the experiments. Differences in precipitation in the MC region between the control and melting experiments and opposite changes in oceanic regions to the east and west are linked through changes in the Walker circulation, making it unclear which region is most influential for forcing the improvement in the pattern of precipitation biases. Sensitivity experiments that artificially enhance convection in one region through imposition of sea-surface temperature anomalies produce a negative precipitation response in the other region.

Key Words: convective heating profile; melting layer; weak temperature gradient; tropical variability; Maritime Continent; tropical rainfall bias

Received 21 November 2016; Revised 3 July 2017; Accepted 11 September 2017; Published online in Wiley Online Library

1. Introduction

Previous studies have demonstrated that the process of melting has important consequences for tropical thermodynamic profiles and cloud populations. For example, soundings taken from the tropical western Pacific warm-pool region during Tropical Ocean–Global Atmosphere programme Coupled Ocean–Atmosphere Response Experiment (TOGA COARE) show that the direct effects of melting produce anomalously cool and moist conditions at and slightly below the 0 °C isotherm altitude with warm and dry conditions immediately above this level, resulting in a stable layer (Johnson *et al.*, 1996). Dry air intrusions from the subtropics also occur at such layers, with radiative feedbacks contributing to the vertical thermal structure (Mapes and Zuidema, 1996). Further study on COARE observations by Johnson *et al.* (1999) reveals that the zero-degree stable layers are inferred to inhibit cloud growth and promote cloud detrainment, restricting the vertical extent of congestus clouds to just above the zero-degree level.

Given the important impacts of the melting level on the thermodynamic and cloud structure of the Tropics, realistic representation of melting processes in general circulation models (GCMs) is important for realistic simulation of tropical climate and its variability. Sud and Walker (2003) studied the influence of melting/freezing physics on simulated cumulus convection in a global model. Their study highlighted the fact that since moist convection is strongly linked to ice-phase physics, its neglect or inadequate treatment is a potential cause of GCM deficiencies. By including melting and freezing physics in their convection parametrization, tropical rainfall bias in their model was reduced.

The Met Office Unified Model (UM: Walters *et al.*, 2011) has melting/freezing physics included in the parametrized convection scheme. In the UM, melting or freezing occurs when hydrometeors cross the freezing level, which is set to be 273 K. Convective heating and moisture profiles indicate that the UM has a narrow, high-amplitude cooling and drying spike at the freezing level (Zhu and Hendon, 2015) due to all falling snow being melted within the layer where the environmental temperature reaches

freezing. The freezing level is only represented by one model level in the high vertical resolution model. However, observations suggest that a mix of frozen and liquid precipitation exists over a layer several hundred metres deep from the freezing level downwards (Johnson *et al.,* 1996; Illingworth and Thompson, 2011). We will assess whether changing the depth over which melting occurs affects the simulation of tropical climate in the UM. A simple way to alter the convection scheme to test this sensitivity is to allow a mix of liquid and frozen precipitation from the freezing level to a lower layer that is 3 K warmer. This change allows a mix of snow and rain to exist over a deeper layer with the proportion of rain increasing linearly from zero at the freezing level to one at the layer with temperature equal to 3 °C.

Our experiments are motivated by the need to reduce tropical precipitation biases in the Maritime Continent (MC) and surrounding regions in the UM. The MC includes the archipelago consisting of Indonesia, New Guinea and Malaysia, and the surrounding shallow seas. It is located within the climatological Indo-Pacific warm pool, a region associated with sea-surface temperatures (SSTs) higher than ∼28 °C, where widespread convective activity (e.g. Keenan *et al.,* 2000) contributes to the rising branch of the Walker circulation. Convective activity in the MC is closely related to large-scale variations in the climate system in both the Tropics and high latitudes (Neale and Slingo, 2003). Despite its global importance, the MC is a region where global climate models struggle to realistically represent the spatial distribution of rainfall and its variability (Jourdain *et al.,* 2013). Simulations with a climate version of the Met Office model (Neale and Slingo, 2003) indicate large negative precipitation biases over the MC region. Errors persist even in higher-resolution simulations of the same model, indicating deficiencies in the representation of the physical system. It is further argued that deficient rainfall over the MC could be a driver for other systematic errors, such as the excess precipitation over the western Indian Ocean. The MC dry bias has been persistent in recent global versions of UM, including the latest versions GA6 and GA7 (Walters *et al.,* 2017 and Walters *et al.* 2017; submitted). Biases in rainfall over the MC region have also been reported to adversely affect simulation of the eastward propagation of the Madden–Julian Oscillation (MJO) across the region (e.g. Neale and Slingo, 2003; Klingaman and Woolnough, 2014).

An aim of this work is to understand how and why changes to the treatment of melting influence the dry bias over the MC region in the UM. We will employ a diagnostic analysis to the UM to help understand the physical impact of melting layer variations that relies on the well-known fact that the tropical atmosphere is characterized by weak horizontal temperature gradients (WTG) on synoptic scales (e.g. Charney, 1963; Sobel and Bretherton, 2000). We will diagnose how changes in the treatment of melting affects diabatic heating profiles, which recent studies have highlighted as being important to tropical climate (e.g. Schumacher *et al.,* 2004; Chikira, 2014; Yokoi, 2015). We will employ techniques recently developed by Chikira (2014), who used WTG balance to understand moistening processes responsible for maintaining MJO convection and how they relate to diabatic heating variations. In particular, the smallness of the Coriolis parameter on the Equator implies a dominant thermodynamic energy balance between adiabatic cooling and diabatic heating. For a given diabatic heating, a vertical velocity required to maintain the dominant thermodynamic balance can be determined if static stability is known. The effects of vertical moisture advection associated with this balancing vertical velocity (which is highly sensitive to the details of the diabatic heating profile) and direct removal of sources of moisture associated with physical parametrizations can then be assessed in terms of their ability to maintain tropospheric moisture anomalies that are favourable for convection. We will show below that changing the treatment of melting in UM modifies the diabatic heating profile in such a way as to make the MC region more favourable for convection by favouring more efficient large-scale vertical advective moistening that helps to maintain moisture anomalies. This diagnostic analysis will also highlight that oceanic regions to the east and west of the MC become less favourable for convection due to changes in the heating profile, which may engender an opposite change over the MC through adjustment of the Walker circulation.

We will also show that such changes engender a significant improvement of MJO activity in the model. Our analysis assumes that increasing moisture in the lower to middle free troposphere is favourable for convection by suppressing the ability of dry air entrainment to negatively affect the buoyancy of convecting plumes (e.g. Sahany *et al.,* 2012). Recent studies by Zhu and Hendon (2015) and Klingaman and Woolnough (2014) showed that UM convection is sensitive to free tropospheric humidity and by increasing the convective entrainment rates in UM, the model MJO was improved. A recent analysis by Schiro *et al.* (2016) supports the relevance of free tropospheric humidity to convection over both tropical ocean and land regions.

Our analysis assumes that WTG assumptions and balance can provide insight into the time-mean tropical precipitation distribution in the UM. Previous studies have successfully used WTG assumptions to study time-mean convective distributions in the Tropics associated with phenomena like the Walker circulation (e.g. Bretherton and Sobel, 2002), and so we feel that this assumption is justified. We note however that not all aspects of time-mean tropical precipitation may be captured using our diagnostic method. For example, regions of time-mean precipitation near coastlines may be strongly influenced by the propagation of diurnally varying precipitation features, for which regulation by free-tropospheric humidity is less important (e.g. Bergemann and Jakob, 2016). We note that the precipitation changes experienced in this study when modifying the treatment of melting are largely oceanic rather than coastal or over land, and so we anticipate our diagnostic method will be largely successful at diagnosing the reasons for these oceanic changes.

This article is organized as follows. The UM and implementation of the melting-level sensitivity test are described in section 2. Basic analysis of the model mean state, MJO activity, and their biases are discussed in section 3. In section 4, we present the moisture budget diagnosis using the WTG approximation to document how melting-level changes affect the mean precipitation distribution. Conclusions and discussion are contained in the final section.

2. Model description

The UK Met Office Unified Model (UM) with GA2.0 model physics is used in this study (Zhu and Hendon, 2015). The model horizontal resolution is 1.875° by 1.25° with 85 vertical levels, and the integration time step is 1200 s. The model uses a modified mass flux convection scheme based on Gregory and Rowntree (1990). Diagnosis of whether conditions are suitable for convection is based on an undiluted parcel ascent from near the surface. A diagnosis is used to determine whether convection is possible from the boundary layer and, if so, whether the convection is deep or shallow depending on the level of the cloud top. The mid-level convection scheme operates on any instability found in a column above the top of the deep/shallow convection or above the boundary layer in columns where the surface layer is stable. For deep convection, the cloud-base mass flux is calculated based on the reduction to zero of convective available potential energy (CAPE) over a given time-scale. The CAPE closure has been modified in various ways to try to address model stability problems (grid-point storms). W-based CAPE closure is the option used in most model configurations. In this scheme, if the maximum large-scale vertical velocity, evaluated before convection, is larger than the threshold vertical velocity, the CAPE time-scale is reduced to remove the convective instability faster. For deep convection, convective entrainment rates use prescribed profiles. The entrainment coefficient is set to be 1.35

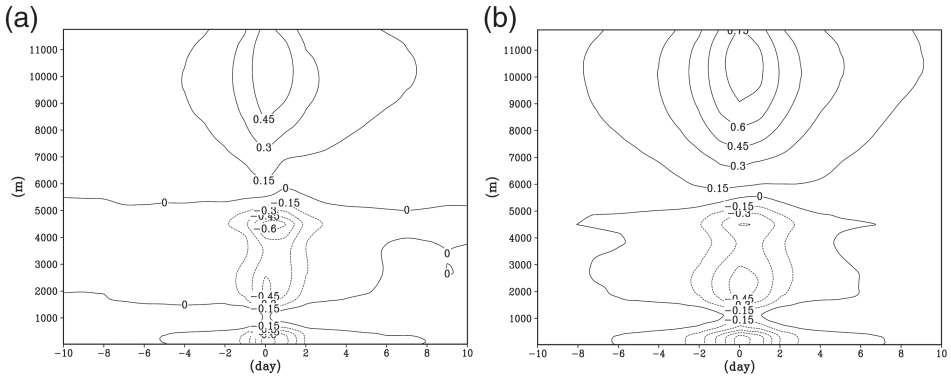

Figure 1. Temperature anomaly (K) relative to the heavy rainfall events (60°E–180°E, 20°S–20°N). (a) Control experiment, (b) Expt. 1.

as in Zhu and Hendon (2015). Mixing detrainment rates depend on relative humidity, and an adapted detrainment scheme is used to calculate the forced detrainment rates. The representation of convective momentum transports (CMT) is based on an eddy viscosity model, and a flux gradient approach has been introduced in the latest version of the model. A downdraught scheme based on Gregory and Allen (1991) is included.

The model uses the prognostic cloud fraction and prognostic condensate (PC2) scheme of Wilson *et al.* (2008). For the boundary-layer scheme, turbulent fluxes of heat, moisture and horizontal momentum in the boundary layer are represented by a first-order K-profile closure as described by Lock *et al.* (2000). Model radiation is represented by a modified version of the Edwards and Slingo (1996) scheme based on rigorous solution of the two-stream scattering equations including partial cloud cover.

The model simulations use observed weekly SST and sea ice distributions, and the simulations cover the period from 2006 to 2009. Two experiments are carried out in this work, a control experiment and a melting-layer sensitivity experiment we call Expt.1. In the standard version of UM, due to the high vertical resolution, the freezing level is only represented by one model level, which is the first model level at which falling frozen hydrometeors reaches 0 °C temperature. As mentioned in the introduction, a simple way to alter the convection code is to allow a mixture of liquid and frozen precipitation from the freezing level to a lower layer that is 3 K warmer. This change allows a mix of snow and rain to exist over a deeper layer with the proportion of rain increasing linearly from zero at the freezing level to one at the layer with temperature equal to 3 °C. The simulation with this modified treatment of melting will be referred to as Expt. 1.

3. Model results

To show the temperature profile associated with intense warm-pool convection, we generate height versus lag composites of temperature relative to the time of the maximum rainfall anomaly for Indo-Pacific warm-pool locations (Figure 1). At each grid point, we define a heavy rainfall event as the occurrence of a rainfall anomaly that exceeds one standard deviation, which average 9.52 and 9.62 mm day^{-1} for the control experiment and Expt. 1 respectively. Here we calculate anomalies by removing the climatologically seasonal cycle over the 4-year simulations.

At the time of maximum precipitation in the control simulation, a positive temperature anomaly that maximizes near an amplitude of 0.45° occurs at 10 km, associated with diabatic heating in the upper troposphere. Meanwhile, cold temperature anomalies occur in the lower troposphere at day 0, likely a result of rain evaporation. This profile at day 0 is consistent with top-heavy diabatic heating resulting from stratiform precipitating systems (Houze, 1989, 1997). A cold spike exists at 4.5 km with a minimum near −0.6 K. This cold spike is associated with melting snow at the freezing level that leads to a strong single-level cold anomaly. In Expt. 1, the cold anomaly at the time of maximum rainfall rate has been reduced by about 0.3 K (Figure 1(b)) relative to the control. The cooling maximum is now located in the lower troposphere, at about 2.3 km, instead of in the middle troposphere. The result from Lin *et al.* (2004, their figure 5) shows that the stratiform heating profile from observations has the maximum cooling rates around 750 hPa, at an elevation of about 2.5 km.

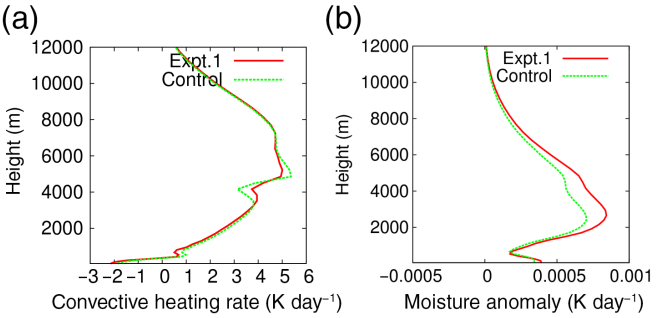

Figure 2. The comparison of (a) the convective heating rate (K day^{-1}) and (b) moisture anomaly (kg kg^{-1}), averaged for 20 days for the time range shown in Figure 1. The green dashed line is for the control experiment and the red solid line is for Expt. 1. [Colour figure can be viewed at wileyonlinelibrary.com].

To show the impact of the modified melting-layer treatment on the heating rate, Figure 2(a) plots the control and Expt.1 convective heating rate averaged between −10 day and +10 day lags for the same events as in Figure 1. For the control experiment, a zig-zag pattern of convective heating rate exists near the melting layer, with a warming peak above and a cooling peak below the melting layer. The cooling peak is associated with the melting being concentrated in one layer and the warming peak is likely associated with extensive cloud tops near the freezing level (Johnson *et al.*, 1999). It is evident that by increasing the melting depth, cooling associated with melting immediately below the freezing level has been reduced. Meanwhile, the warming peak above is also reduced. It is also apparent that Expt. 1 has modestly reduced warming rates throughout the lower troposphere below 3000 m.

Figure 2(b) also shows that precipitation events with modified melting treatment are associated with a moister troposphere. This effect is particularly pronounced over the MC region, to be discussed below. One effect of such a signal would be to reduce long-wave radiative cooling to space per unit precipitation, with the effect it has on the moisture budget discussed in more detail in the next section. While it is not entirely clear why the troposphere, especially in the lower half, is moister by changing the treatment of melting, it is possible that the reduced cooling spike at the melting level has a direct impact on detrainment rates. This may affect the amount of condensate that is detrained and falls into the lower troposphere. While there is a direct moistening of the lower troposphere caused by condensate evaporation, Chikira (2014) argues that the evaporative cooling that results would be balanced by downward motion and hence drive a negative moisture advection that would overwhelm the direct moistening effect. In our melting experiment, such drying processes would

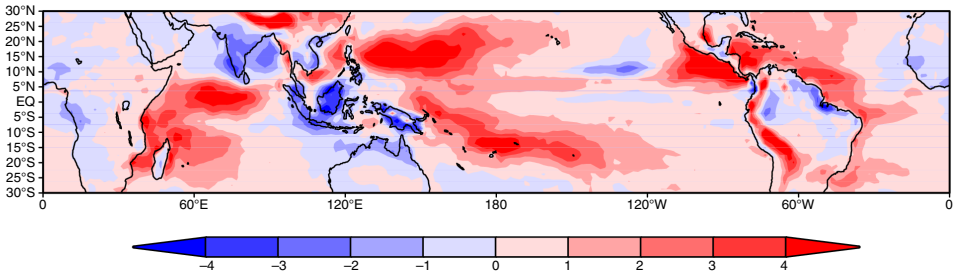

Figure 3. The model bias of precipitation rate (mm day^{-1}) of the control experiment compared to the GPCP observation, averaged for the four years 2006–2009. [Colour figure can be viewed at wileyonlinelibrary.com].

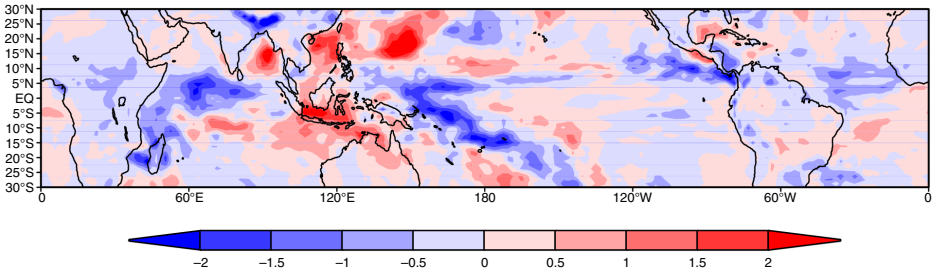

Figure 4. The averaged rainfall rate (mm day^{-1}) difference between Expt. 1 and the control experiment. [Colour figure can be viewed at wileyonlinelibrary.com].

be reduced. An analysis of detrainment rates indicates that these are reduced in the melting experiments, consistent with this argument (not shown).

Figure 3 shows the 4-year averaged rainfall bias in the control experiment compared with Global Precipitation Climatology Project (GPCP) observations. A tri-polar pattern to the rainfall bias exists. The precipitation bias is characterized by positive precipitation biases in the west and central Indian Ocean and western Pacific Ocean. In between the positive biases, a negative precipitation bias exists in the MC and northern Australia. A dry bias also exists in the Indian monsoon region. Biases in a given hemisphere are most pronounced during the local summer, with biases in the MC region most evident in December–February. Also of note is the positive precipitation bias that exists in the warm pool of the western Atlantic and east Pacific.

The averaged rainfall rate differences between Expt. 1 and the control experiment are shown in Figure 4. The difference between the two experiments has the opposite sign to the model bias of the control experiment. The averaged rainfall rate is increased in the MC region and northern Australia where the control simulation has a dry bias, and wet biases are reduced in the Indian Ocean and west Pacific warm pool regions to the west and east, respectively. The rainfall biases are not completely alleviated, and the maximum bias reduction is in the oceanic regions of the MC between Borneo and Java. The bias reduction is strongest during December–February, when mean biases in this region are greatest. We hypothesize that the pattern of bias reduction shown in Figure 4 is related to changes of the lower tropospheric heating profile with the change in melting, which is explored in more depth in the next section. Rainfall biases in the east Pacific warm pool are also improved with changes to the treatment of melting. It is worthy of note that the wet bias over the northwest Pacific is worsened in Expt.1, which we will investigate in a future study. In this work, we mainly focus on model bias in the deep Tropics, where WTG assumptions used in the diagnostic analysis below are most applicable for diagnosing precipitation biases.

With the improvement of the mean precipitation distribution in the MC, the eastward propagation of organized convection associated with MJO has also been improved. To demonstrate the ability of the model to simulate eastward-propagating intraseasonal variability, we calculate the lead–lag correlation coefficients between 20 and 100 days bandpass filtered data from a central Indian Ocean time series and the associated 10°N–10°S averaged fields at all longitudes (Figure 5). For the control experiment, convection fails to propagate eastward from the Indian Ocean. Further, 850 hPa zonal wind does not show organized eastward propagation. In Expt. 1, with the improvement of the mean precipitation distribution in the MC region, the model exhibits improved eastward propagation across the Indian and the west Pacific Oceans. Chikira (2014) used moistening diagnostics based on WTG theory to argue that the ability to destabilize the MJO is strongly dependent on the details of the vertical heating profile, including changes to the treatment of melting and freezing. We will use such diagnostics below to explain why conditions become generally more favourable for supporting convection in the MC region, although these diagnostics may also provide complementary information on why MJO destabilization is also favoured in the MC region with an improved treatment of melting.

The simulation of the MJO in the two models is quantified using wave-number–frequency co-spectral analysis (e.g. Hendon and Wheeler, 2008) in Figure 6. The analysis is applied to daily mean outgoing long-wave radiation (OLR) and zonal wind at 850 hPa (U850), and, to focus on the MJO, we display the coherence and phase spectrum for the equatorially symmetric components (e.g. Wheeler and Kiladis, 1999). The observed MJO is characterized by a distinct peak in coherence squared between OLR and U850 of about 0.6 at zonal wave-number 1–2 and ∼50-day period (Hendon and Wheeler, 2008). We can see a clear peak in coherence spectrum in the 30–80-day band at zonal wave-number 1 in Expt.1 and little evidence of any similar peak in the control experiment (Figure 6), confirming the MJO simulation is improved in Expt.1.

4. Moisture budget diagnosis under WTG balance

Chikira (2014) used WTG balance to investigate the maintenance of moisture anomalies in MJO convective regions, under the assumption that high lower-to-middle free tropospheric moisture is crucial to supporting MJO convection. Details of the lower-to-middle tropospheric diabatic heating profiles affected by melting/freezing, rain evaporation and radiation were demonstrated to sensitively affect the ability of a GCM to support the moisture anomalies that maintain MJO convection. In this section, we use similar moisture budget diagnostics under the WTG assumption to investigate why Expt.1 is able to sustain higher mean-state precipitation in the MC region than in the control version of UM, and lower mean precipitation in oceanic regions to the west and east.

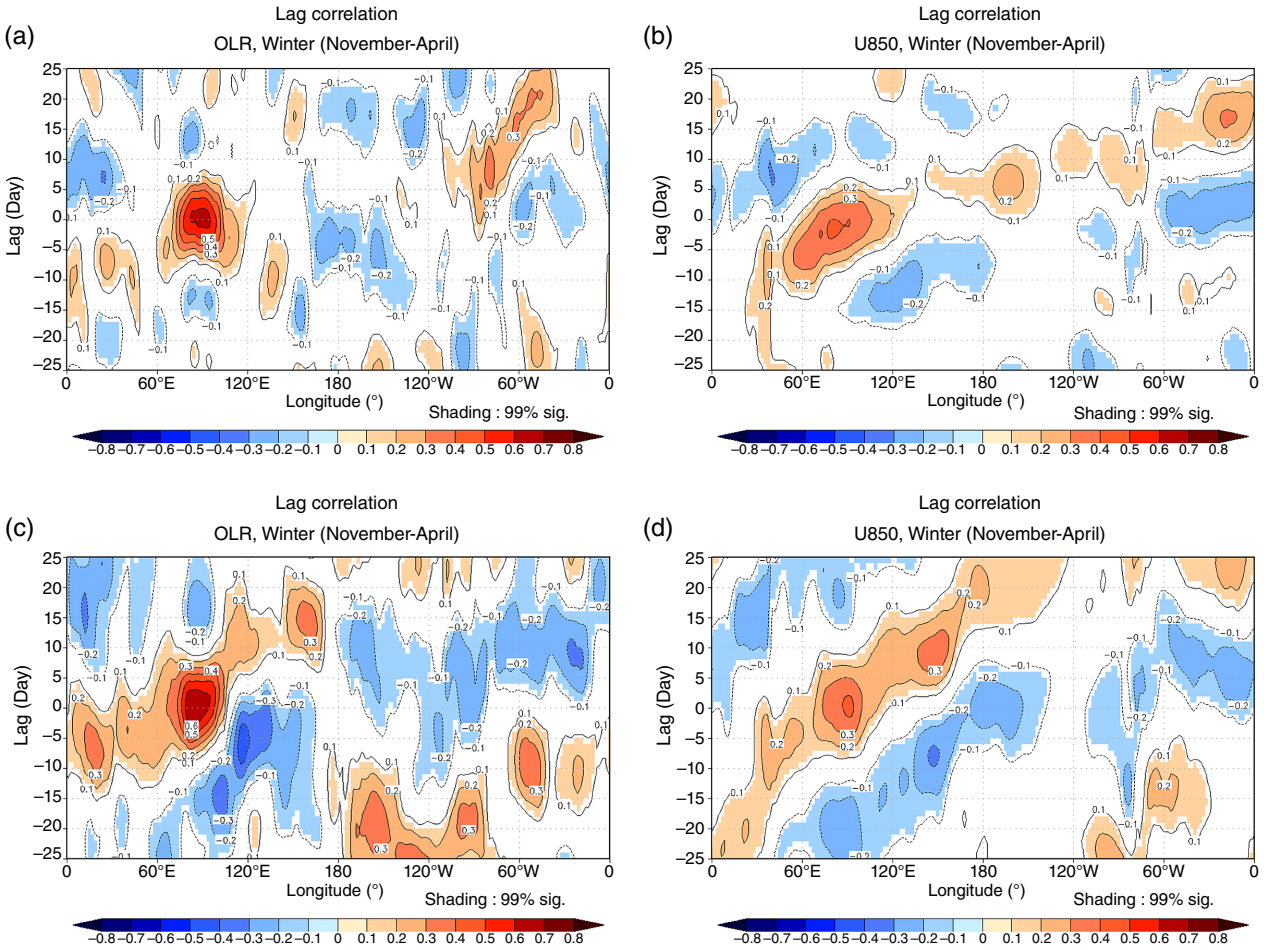

Figure 5. Lag correlation of equatorial intraseasonal OLR (a, c) and 850 hPa zonal wind (b, d) onto a reference time series at 90°E. The upper panels are for the control experiment (a, b) and the lower panels are for Expt. 1 (c, d). [Colour figure can be viewed at wileyonlinelibrary.com].

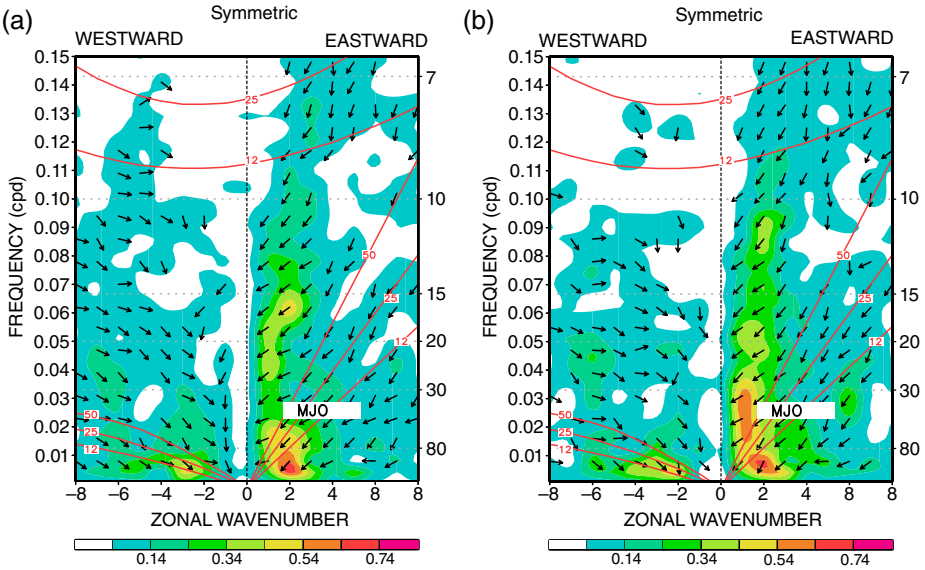

Figure 6. Coherence squared (colours) and phase (vectors) spectrum between the symmetric OLR and U850 for (a) control experiment and (b) Expt.1. Upward-pointing arrows indicate that the fields are in phase, and an arrow pointing to the right indicates that the first field is leading the second field by a quarter cycle. Superimposed are the dispersion curves of the equatorial waves for the equivalent depths of $h = 12$, 25 and 50.The coherence and phases spectrum was computed by first averaging power and cross power using 256-day segments that were overlapped by 50 days. [Colour figure can be viewed at wileyonlinelibrary.com].

By assuming that the tropical atmosphere is characterized by weak spatial gradients in temperature on intraseasonal and longer time-scales, the thermodynamic energy equation can be simplified to first order, following Charney (1963), to

$$\omega \frac{\partial s}{\partial p} = Q, \tag{1}$$

where Q includes the diabatic heating sources for the troposphere from model physics, including apparent heating from convection, heating rates from the large-scale precipitation and radiative heating/cooling rates. s is the dry static energy and ω is the vertical velocity in pressure coordinates.

Based on Eq. (1) and as described in Wolding and Maloney (2015) and Zhu and Sobel (2012), we can generate a vertical velocity to balance an apparent heating,

$$\omega_{\mathrm{WTG}} = Q\left(\frac{\partial s}{\partial p}\right)^{-1}. \tag{2}$$

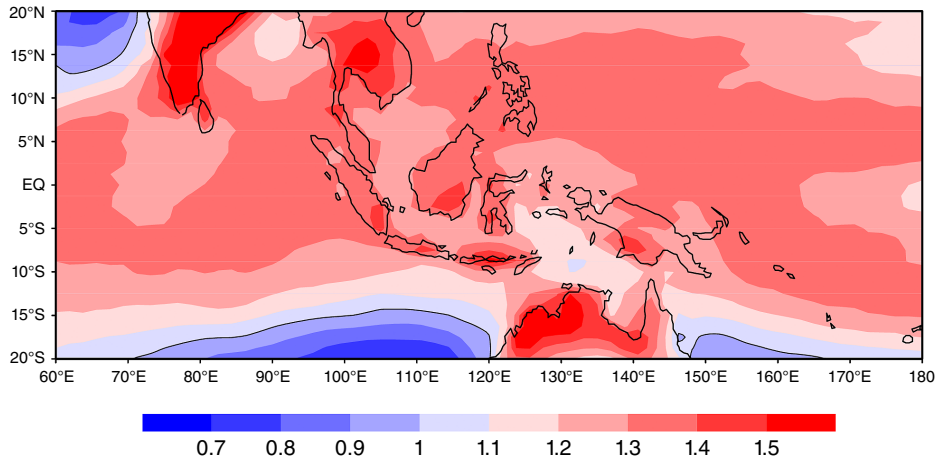

Figure 7. Annual-mean alpha (α) averaged from 850 to 600 hPa calculated from the monthly-mean s and q in the model. [Colour figure can be viewed at wileyonlinelibrary.com].

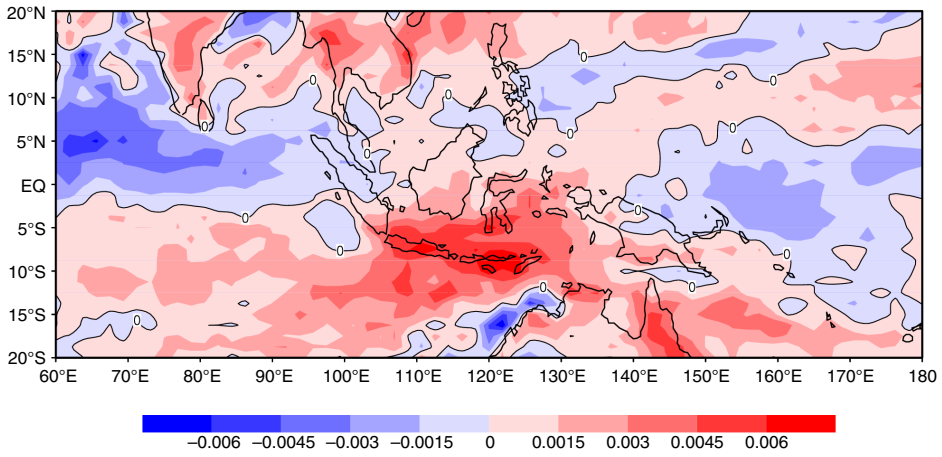

Figure 8. $\Delta(\overline{\alpha\widehat{Q}})$ integrated from 850 to 600 hPa between Expt. 1 and the control experiment. [Colour figure can be viewed at wileyonlinelibrary.com].

At long time-scales, Wolding and Maloney (2015) showed that this prediction of vertical velocity is a good approximation. Then, ω_{WTG} can drive a latent heat advection,

$$-\omega_{\mathrm{WTG}}\frac{\partial Lq}{\partial p} = -Q\left(\frac{\partial s}{\partial p}\right)^{-1}\frac{\partial Lq}{\partial p}, \tag{3}$$

which can also be written as

$$-\omega_{\mathrm{WTG}}\frac{\partial Lq}{\partial p} = Q\alpha. \tag{4}$$

The parameter α is defined as

$$\alpha = -L\left(\frac{\partial s}{\partial p}\right)^{-1}\frac{\partial q}{\partial p}. \tag{5}$$

The parameter α (Chikira, 2014; Wolding and Maloney, 2015) is essentially a measure of how efficiently an apparent heating Q can drive a moisture tendency through vertical advection under WTG balance. The variable α is the ratio of the vertical moisture gradient and a measure of the static stability, with the latter determining the amount of vertical motion required to balance an apparent heating and the former determining the amount of moistening that results from the required vertical motion given the vertical moisture gradient.

Figure 7 shows the annual-mean α averaged over the lower troposphere (850 to 600 hPa) calculated from monthly-mean s and q, consistent with Chikira (2014), in the control simulation for the region of the Indian Ocean and west Pacific. As shown in Figure 7, α is larger than 1 on average in the lower troposphere in the Tropics. Moreover, it has the largest values over the MC, particularly over land regions. We also note that oceanic regions of the west Pacific and Indian Ocean warm pools also have higher α than the inland seas of the MC. Regions of higher α are associated with stronger vertical moisture advection per unit diabatic heating, and parametrization modifications that change the vertical heating profile in these regions will have a larger impact on moistening that regulates convection. For example, for a given amount of lower tropospheric change in Q, a larger value of α will have larger impacts on moisture vertical advection according to Eq. (4), through αQ. In this way, the large values of α over the MC and the land of northern Australia may help support the local negative precipitation bias shown in Figure 3, if the diabatic heating profile due to parametrization choices is characterized by insufficient positive diabatic heating in the lower troposphere per unit convection. We note however that precipitation changes in the MC region between the control and Expt.1 are most pronounced over the inland seas and not land. Given the higher α over the Indo-Pacific warm-pool regions to the east and west than in the MC inland seas, it is possible that reductions of precipitation biases over those warm-pool regions could be indirectly affecting precipitation in the MC region through changes to the Walker circulation. We will discuss both of these possibilities below.

To demonstrate the role of αQ in producing precipitation changes between the simulations, Figure 8 shows the difference of the time-averaged lower tropospheric αQ (can be written as $\Delta(\overline{\alpha\widehat{Q}})$) between Expt. 1 and the control experiment. Following Chikira (2014) and consistent with WTG theory, we use slow variations of s and q (bandpass filtered to periods greater than 20 days) to calculate the value of α. The heating rate associated with model physics is also normalized by the column-integrated

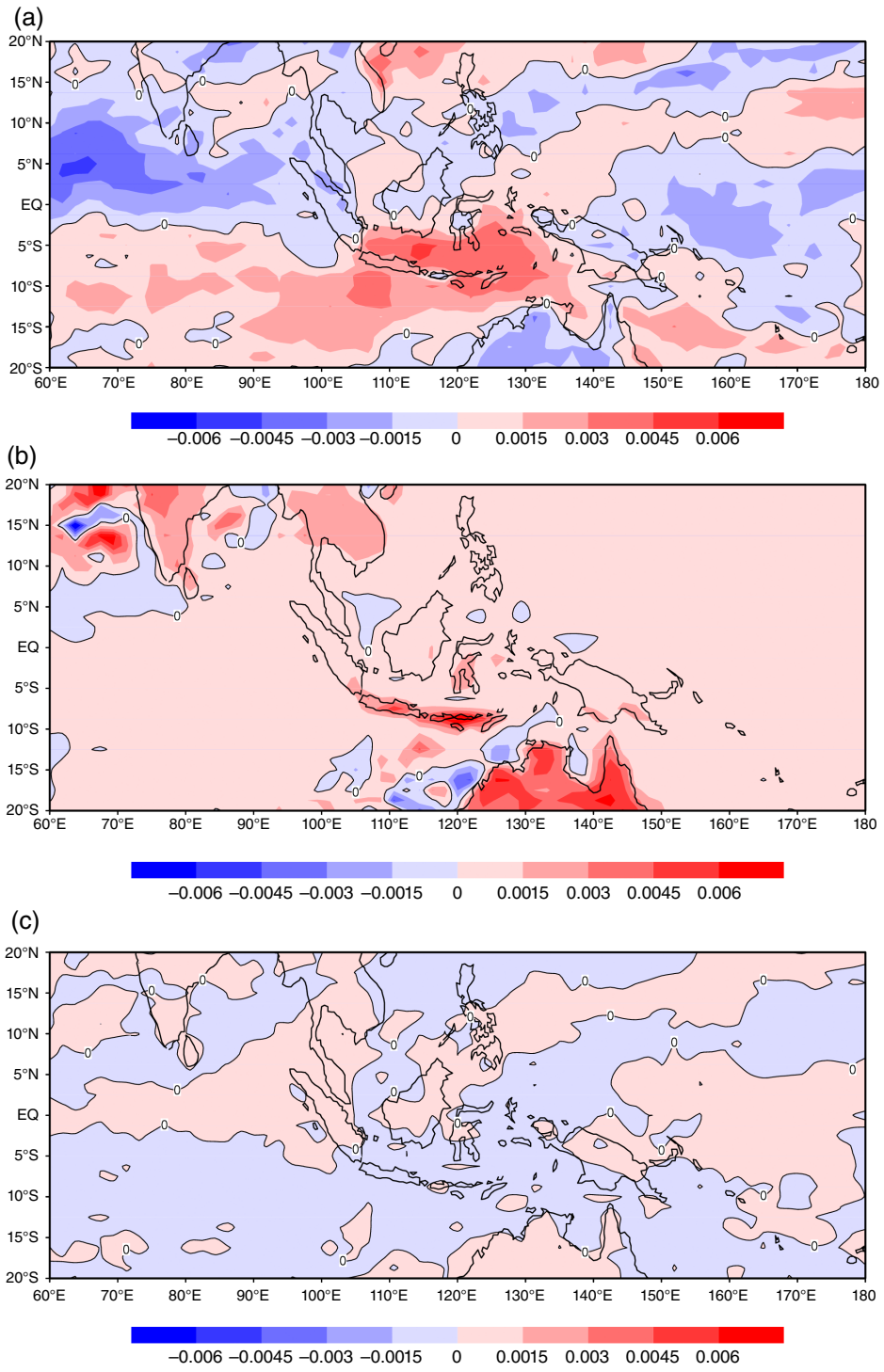

Figure 9. (a) ($\bar{\alpha}\Delta\widehat{Q}$), (b) $\overline{\widehat{Q}}\Delta\alpha$ and (c) $\Delta\alpha\Delta\widehat{Q}$ averaged between 850 and 600 hPa. Δ represents the difference between Expt. 1 and the control experiment. [Colour figure can be viewed at wileyonlinelibrary.com].

convective heating rate for the troposphere to represent the heating rate per unit of column-integrated convective heating, as shown in Eq. (6):

$$\widehat{Q} = \frac{Q}{[Q_{\text{conv}}]}, \tag{6}$$

where $[Q_{\text{conv}}]$ represents the column-integrated convective heating rate over the troposphere, from 850 to 200 hPa.

In Figure 8, a positive value of $\Delta(\overline{\alpha\widehat{Q}})$is observed in the MC region and surrounding seas, generally where rainfall increases in Expt.1 versus the control. Decreases in $\Delta(\overline{\alpha\widehat{Q}})$occur in Indian and west Pacific oceanic warm-pool regions to the east and west, generally coincident with decreases in precipitation between the experiments shown in Figure 4. As will be described below, in the MC region, increased lower tropospheric diabatic heating per unit vertically integrated convective heating supports more moistening in Expt.1 relative to the control and supports increased rainfall there. Conversely, lower tropospheric diabatic heating per unit convective heating will be shown to decrease in the oceanic regions to the east and west, supporting reductions in $\alpha\widehat{Q}$ in those regions.

The time-averaged difference of $\alpha\widehat{Q}$ between the two experiments can be further partitioned as

$$\Delta\overline{(\alpha\widehat{Q})} \approx \overline{\alpha}\Delta\widehat{Q} + \overline{\widehat{Q}}\Delta\alpha + \Delta\alpha\Delta\widehat{Q}. \tag{7}$$

The first term on the right-hand side of Eq. (7) is the effect of the change of normalized heating rate acting on the control simulation time-mean α, the second term represents the change

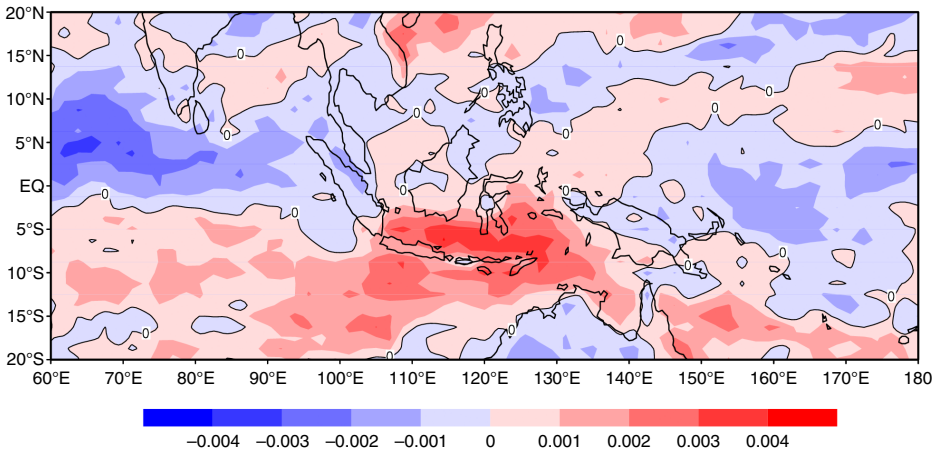

Figure 10. The difference of the averaged ($\Delta\overline{\widehat{Q}}$) between 850 and 600 hPa for Expt. 1 and the control experiment. [Colour figure can be viewed at wileyonlinelibrary.com].

of α acting on the control simulation time-mean normalized $\widehat{Q}$, and the third term represents the nonlinear product. These three terms on the right-hand side of Eq. (7) are shown in Figure 9. It is evident that the $\overline{\alpha}\Delta\widehat{Q}$ term (Figure 9(a)) has the largest contribution to the pattern of Figure 8, and qualitatively matches the precipitation changes in Figure 7(b), especially for the region of maximum bias reduction in the oceanic regions of MC between Borneo and Java, and for the Indo-Pacific Ocean regions to the east and west of the MC. The second term in Eq. (7) represents the change of parameter α acting on the climatological normalized heating rates from the control simulation. Figure 9(b) shows that $\overline{\widehat{Q}}\Delta\alpha$ is positive over the land of the MC region and northern Australia, which would act to enhance local convective activity over land. Decreased static stability appears largely responsible for this change in α between runs. Chikira (2014) showed that localized variations in lower tropospheric static stability were relatively prominent over land regions of the MC. The change associated with the nonlinear advection term (Figure 9(c)) is negligible here compared to the first two terms, and will not be further discussed.

We note that the more generally favourable conditions for convection in the MC make the propagation of MJO convection into that region more likely, consistent with Figure 5. In particular, changing the treatment of melting in UM modifies the diabatic heating profile in such a way as to make the MC region more favourable for convection on all time-scales by favouring more efficient large-scale vertical advective moistening per unit column-integrated diabatic heating that helps to maintain moisture anomalies.

To demonstrate the pattern of the heating rate ($\widehat{Q}$) change, Figure 10 shows the difference of the lower tropospheric Q normalized by the column-integrated convective heating rate between the two experiments. In regions with increased rainfall, making the modification to the treatment of melting is associated with a net increase of the lower tropospheric heating rates per unit of the column-integrated convective heating rate, or a more bottom-heavy heating profile. A change in the opposite sense occurs over the oceanic regions to the east and west of the MC.

To understand the contributions from different model physics to Figure 10, in Figure 11 we plot the averaged model-to-model difference for the heating rates from radiation (Figure 11(a)), convection (Figure 11(b)) and large-scale precipitation (Figure 11(c)). The same normalization as in Figure 10 has been applied to Figure 11. It is evident that the change of $\widehat{Q}$in Figure 10 mainly comes from the change of radiative heating rates in the two experiments. The contributions of the heating rates from convection and large-scale precipitation are one order smaller compared to that of radiation. As explained in Figure 2(b), changing the melting physics in Expt.1 helps to modulate the vertical moisture profile. Increased tropospheric moisture per unit convection in the MC region may reduce radiative cooling rates in the troposphere, with opposite changes over the oceans to the east and west.

Figure 12(a) compares the specific humidity changes for the MC and west Indian Ocean between Expt. 1 and the control. To exclude the cases of weak convective activity, rainfall events were chosen with rates higher than 2 mm day^{-1}, with profiles averaged for the time period between 10 days before and after the peak rainfall. For the MC region, the tropospheric moisture increases in the experiment with modified melting physics, with the largest increase in the lower troposphere. The increased moisture tropospheric moisture in the MC region likely helps to reduce the local radiative cooling rates per unit convective activity as shown in Figure 11. The moisture change in the western Indian Ocean region has the opposite sign, consistent with the increased local radiative cooling rates. Figure 12(b) shows the comparison of the vertical velocity for the MC and west Indian Ocean between the two experiments. Consistent with Figure 12(a), the increased moisture in the MC region is associated with increased vertical velocity in this region. Consistent with a Walker circulation change, the vertical velocity over the west Indian Ocean region decreases, associated with reduced moisture as shown in Figure 12(a).

To further understand the different behaviour of convection between the MC region and the west Indian Ocean region, similar to Figure 12, Figure 13 compares the changes of $\widehat{Q}$ profiles for these two regions between Expt.1 and the control. Please remember that these are the changes in the heating profiles per unit convective heating.

For the MC region, compared to the control experiment, in Expt.1 $\widehat{Q}$ is increased in the lower troposphere and upper troposphere with a minimum value, about zero, at about 3000 km. This is consistent with Figure 10, which shows the increased lower tropospheric $\widehat{Q}$ in Expt. 1. One hypothesis suggested by this result is that parametrization changes directly affect the diabatic heating profile in the MC region, aiding increased convective activity there, and leading to reduced convection over the ocean region of the western Indian Ocean region through a strengthened Walker circulation. However, the possibility also exists that weakened convection over the west Indian Ocean and west Pacific may help drive precipitation of the opposite sense in the MC through a weakened Walker circulation. This possibility is supported by the fact that α is greater in the Indian Ocean and west Pacific than over the inland seas areas of the MC where precipitation changes are largest between the control and Expt.1 (Figures 6 and 7). $\widehat{Q}$ changes in the west Indian Ocean are also very large compared to those in the MC. In Figure 13, $\widehat{Q}$ is decreased at low levels in the western Indian Ocean region with the maximum decrease at 1.8 km. An intriguing possibility is that spreading melting through

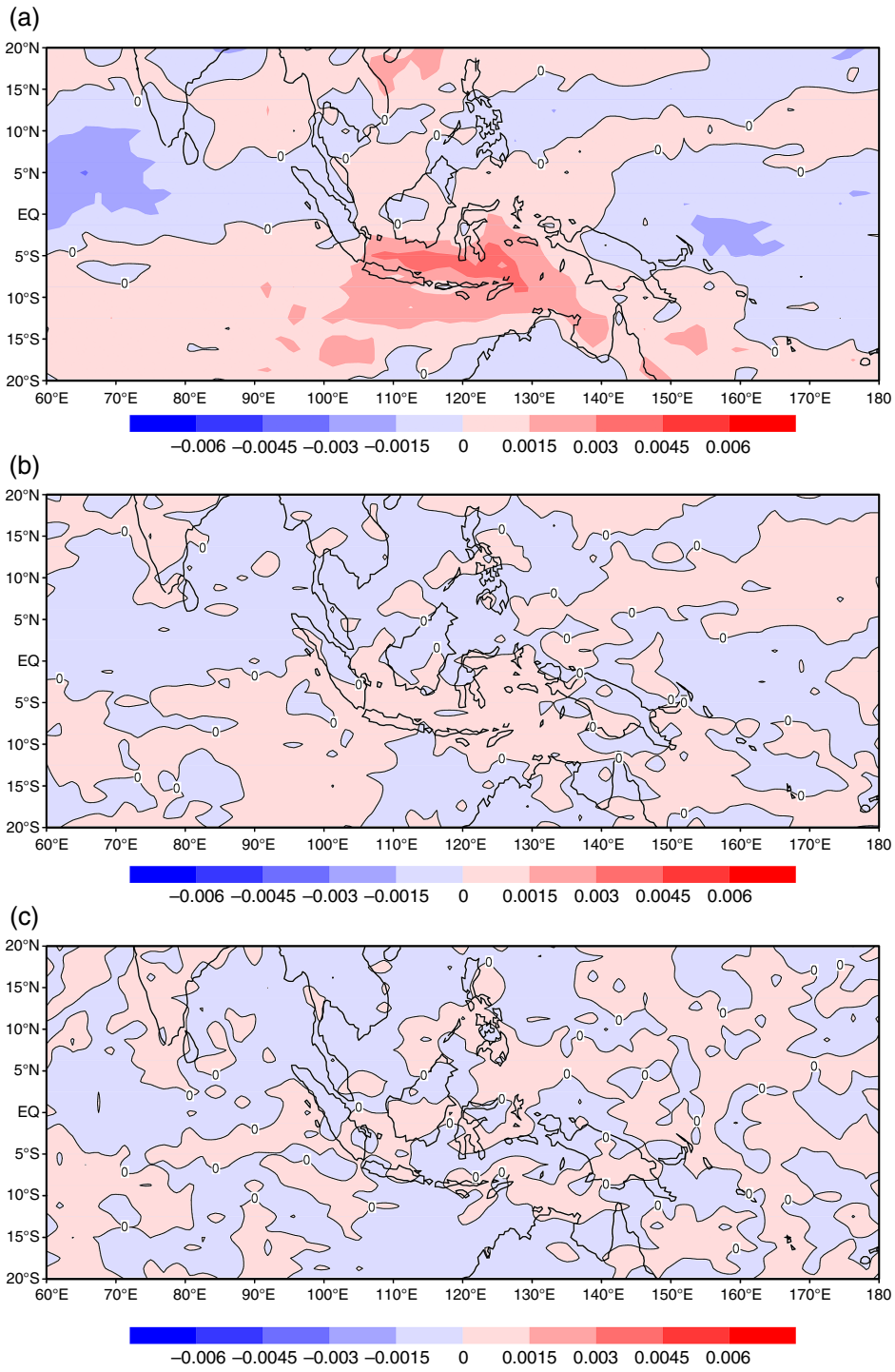

Figure 11. Comparing the normalized heating rate between Expt. 1 and the control experiment from (a) radiative heating rate, (b) convective heating rate, and (c) large-scale precipitation, averaged between 850 and 600 hPa. [Colour figure can be viewed at wileyonlinelibrary.com].

a deeper layer of the lower troposphere in oceanic warm-pool regions locally reduces $\overline{\alpha}\Delta\widehat{Q}$, especially where mean α is relatively high, leading to reduced precipitation and creating a remote response over the MC. The increased lower tropospheric cooling per unit total convective heating in Figure 13 is spread over a deeper layer of the lower troposphere than the direct influence of the melting level change, however.

To support the contention that precipitation changes in one region can have desirable remote impacts elsewhere through modifications to the Walker circulation, we conduct two further sensitivity tests. We carried out two experiments in which SST is increased by 0.3 °C in a patch (i) over the MC and (ii) over the western Indian Ocean. The SST patches used have a longitude span of 2200–3300 km, which is of the same order as the approximately 4000 km longitude scale of forcing used in Gill (1980, 1982) to diagnose the atmospheric flow response to a forcing in a shallow-water system. No other model settings are different from the control experiment. MC precipitation is increased by increasing local SSTs, with a compensating reduction in the wet bias over the western Indian Ocean region (Figure 14(a)). Similarly, increasing SST over the western Indian Ocean increases precipitation there, with a compensating decrease in precipitation in the MC region (Figure 14(c)).To show the response of the circulation changes to the SST changes, we calculated the average vertical velocity changes averaged between 10°S and 5°N. The local ascending motion associated with convection over the MC region is increased by increasing local SSTs, with a compensating subsidence over the western Indian Ocean region and west Pacific region where the model has a wet bias (Figure 14(b)). Similarly, increasing SST over the western Indian Ocean region increases local vertical ascending motion due to the stronger convection, with a compensating subsidence

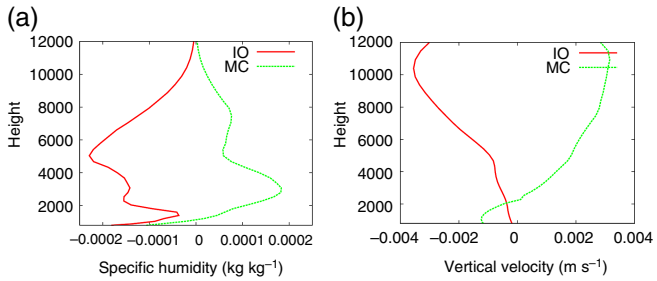

Figure 12. Comparing the difference of (a) the specific humidity ($kg\,kg^{-1}$) and (b) the vertical velocity ($m\,s^{-1}$), between MC (12°S–2°N, 100–130°E, green) and IO regions (3°S–9°N, 60–80°E, red), choosing rainfall events with rainfall rates bigger than 2 mm day^{-1}. The results are averaged between the period of −10 day and +10 day of the peak rainfall. [Colour figure can be viewed at wileyonlinelibrary.com].

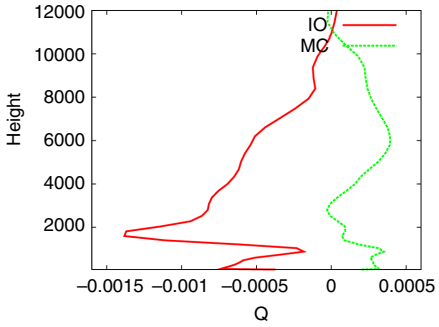

Figure 13. Comparing the difference of the normalized Q between MC (12°S–2°N, 100–130°E, green) and IO (3°S–9°N, 60–80°E, red) regions using all rainfall events with rainfall rates bigger than 2 mm day^{-1}. The results are averaged between the period of −10 day and +10 day of the peak rainfall. [Colour figure can be viewed at wileyonlinelibrary.com].

in the MC region (Figure 14(d)). These experiments support the contention that physical parametrization changes that positively affect the convection in one region can have beneficial effects at reducing bias elsewhere through an adjustment of the large-scale circulation.

5. Conclusion and discussion

The control version of the UM has a large cooling spike at the freezing level due to all the snow being melted in one layer where the environmental temperature reaches the freezing level. This model is characterized by dry biases over the MC and positive precipitation biases in tropical oceanic regions to the east and west. By allowing a mixture of snow and rain between the freezing level and the layer that reaches 3 K above freezing, precipitation increases in the MC and northern Australia, and decreases in oceanic regions to the east and west of the MC. As a result, model precipitation bias in the tropical Indian Ocean, MC, and west Pacific region is improved in this simulation with modified treatment of melting. The improved precipitation biases are accompanied by improved eastward propagation of organized convection associated with the MJO.

We used 3 K above freezing to define the base of the melting layer. This value is the average from observational studies (Fabry and Zawadzki, 1995). In Johnson *et al.* (1996), they mentioned that the melting layer is about 500 m deep just below 0 °C. In future studies, we will investigate the sensitivity of results to changes in the depth of melting. We anticipate that the rainfall change pattern will be qualitatively similar to this study, but with slightly increased amplitude for deeper melting levels. In this study, we are using an earlier version of UM with GA2.0 model physics, not the latest version of the Met Office model. The results could be sensitive to this issue because different versions of UM have different model physics packages. It is also worthy to mention that the melting layer problem is due to be fixed in a later UM version with GA8 model physics (A. Stirling, 2017; personal communication).

We have used WTG theory, specifically the diagnostics developed by Chikira (2014) and Wolding and Maloney (2015), to examine the importance of vertical diabatic heating structure changes caused by changes to the treatment of melting for producing lower tropospheric moisture and precipitation changes. The modified melting experiment increases the MC lower tropospheric diabatic heating rate per unit column-integrated convective heating ($\widehat{Q}$), which helps to increase upward lower-tropospheric moisture advection per unit convective heating through the term $\alpha \bullet \widehat{Q}$, making conditions more favourable for convection there. The parameter α (Chikira, 2014; Wolding and Maloney, 2015) is essentially a measure of how efficiently an apparent heating Q can drive a moisture tendency through vertical advection under WTG balance. Lower-tropospheric diabatic heating per unit column-integrated convective heating decreases in the tropical ocean regions of the west Pacific and Indian Ocean in the modified melting experiment, decreasing upward lower-tropospheric moisture advection per unit convective heating through the term $\alpha\widehat{Q}$ in those regions, and making conditions less favourable for convection. As a result, the average rainfall rate change between the modified melting experiment and control is well correlated with the average change of αQ. Changes in lower-tropospheric radiative heating per unit convection seem particularly influential in engendering mean precipitation changes between the experiments. To summarize, microphysical changes to the treatment of melting modifies the vertical heating profile in the lower troposphere, which then leads to grid-scale advective moistening anomalies through WTG balance and a modified environment in which convection exists. As noted in section 2, the entrainment rate is set as in Zhu and Hendon (2015) which makes the convection scheme sensitive to moisture in the lower free troposphere, and hence physical changes that effect the treatment of lower-tropospheric moisture entail a response in convection that reduces model precipitation biases. We anticipate the WTG-based mechanism proposed here will work best in oceanic regions in the vicinity of the Equator where the Coriolis force is small and temperature gradients weak, and these arguments to work less well in off-equatorial regions.

Changes in precipitation in the MC region between the control and melting experiments and opposite changes in oceanic regions to the east and west are linked through changes in the Walker circulation. This fact is verified through experiments where SST and precipitation are artificially increased in one region, and opposite-signed precipitation changes are produced in the other region. It remains unclear based on the analysis here which region (MC or oceanic regions to east and west) is most important for driving the pattern of precipitation change between the melting experiment and control simulation. Oceanic values of α are higher in Indian and west Pacific Oceans regions than in the inland seas of the MC, suggesting that convection in the Indian and west Pacific Oceans is more sensitive to parametrization changes that affect the vertical heating profile. These precipitation changes would then force an opposite response over the MC through adjustments to the large-scale circulation. However, the largest values of α in the simulations are located over the islands of the MC, and so it is also possible that precipitation changes in this region could be driving opposite-signed precipitation changes to the east and west through adjustment of the circulation. These topics remain under active investigation.

Although we have emphasized ice melting processes and their impact on the precipitation bias, there are other microphysical processes such as rain autoconversion which may also play an important role in modulating precipitation biases as shown in Golaz *et al.* (2011). However, the UM convection scheme we use here does not include autoconversion. A recent paper by Abhik *et al.* (2017) also shows that better representation of the spatial and vertical distributions of cloud hydrometeors produces more

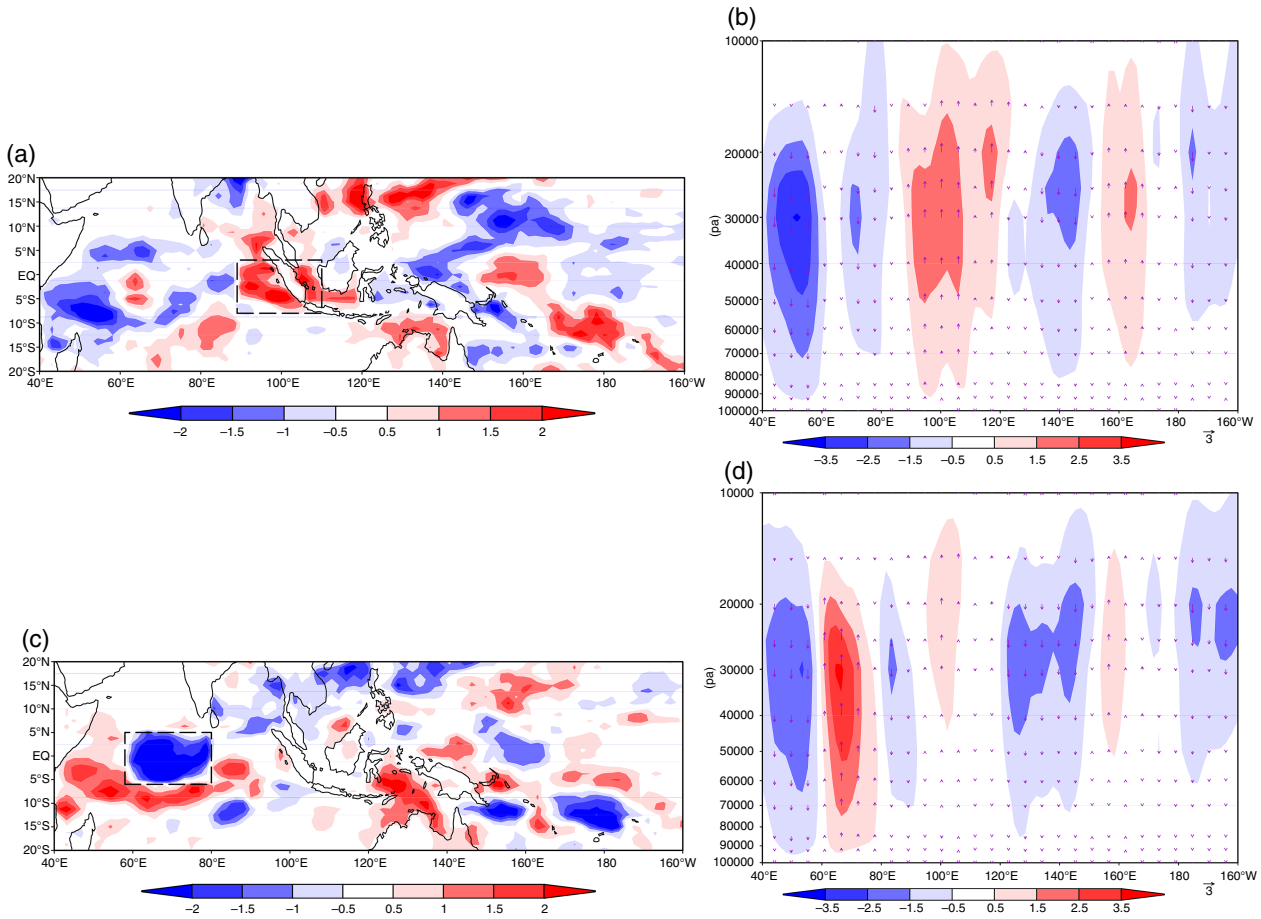

Figure 14. The difference of the precipitation rate ((a, c), unit: mm day^{-1}) and the vertical velocity ((b, d), unit: 10^{-3} m s^{-1}) between the experiments with a local SST change and the control experiment. SSTs increase over the region of MC (90°E–120°E, 5°S–2°N, (a, b)) and IO (60°E–80°E, 5°S–5°N, (c, d)). The thick dashed black lines are for the regions with increased SSTs. The vertical velocity is averaged between 10°S and 5°N. [Colour figure can be viewed at wileyonlinelibrary.com].

realistic propagation of a simulated low-frequency boreal summer intraseasonal oscillation.

Acknowledgements

This research is supported by the Australian Government Department of the Environment, National Environmental Science Programing (NESP) ESCC Hub research project in Australia. E. Maloney acknowledges support by the NOAA MAPP programme under awards NA15OAR4310099 and NA15OAR4310098, and by National Science Foundation (NSF) Climate and Large-Scale Dynamics Program under award AGS-1441916.

References

Abhik S, Krishna RPM, Mahakur M, Ganai M, Mukhopadhyay P, Dudhia J. 2017. Revised cloud processes to improve the mean and intraseasonal variability of Indian summer monsoon in climate forecast system: Part 1. *J. Adv. Model. Earth Syst.* **9**: 1002–1029. https://doi.org/10.1002/2016MS000819.

Bergemann M, Jakob C. 2016. How important is tropospheric humidity for coastal rainfall in the tropics? *Geophys. Res. Lett.* **43**: 5860–5868. https://doi.org/10.1002/2016GL069255.

Bretherton CS, Sobel AH. 2002. A simple model of a convectively-coupled Walker circulation using the weak temperature gradient approximation. *J. Climate* **15**: 2907–2920.

Charney CG. 1963. A note on large-scale motions of the tropics. *J. Atmos. Sci.* **20**: 607–609.

Chikira M. 2014. Eastward-propagating intraseasonal oscillation represented by Chikira–Sugiyama cumulus parameterization. Part II: Understanding moisture variation under weak temperature gradient balance. *J. Atmos. Sci.* **71**: 615–639. https://doi.org/10.1175/JAS-D-13-038.1.

Edwards JM, Slingo A. 1996. Studies with a flexible new radiation code. I: Choosing a configuration for a large-scale model. *Q. J. R. Meteorol. Soc.* **122**: 689–719.

Fabry F,, Zawadzki I. 1995. Long-term radar observations of the melting layer of precipitation and their interpretation. *J. Atmos. Sci.* **52**: 838–851.

Gill AE. 1980. Some simple solutions for heat-induced tropical circulation. *Quart. J. R. Met. Soc.* **106**: 447–462.

Gill AE. 1982. Atmosphere-Ocean Dynamics, *International geophysics theories*, Vol. 30.

Golaz J-C, Salzmann M, Donner LJ, Horowitz LW, Ming Y, Zhao M. 2011. Sensitivity of the aerosol indirect effect to subgrid variability in the cloud parameterization of the GFDL Atmosphere General Circulation Model AM3. *J. Climate* **24**: 3145–3160. https://doi.org/10.1175/2010JCLI3945.1.

Gregory D, Allen S. 1991. 'The effect of convective downdraughts upon NWP and climate simulations'. In *Ninth Conference on Numerical Weather Prediction*, Denver, CO, 122–123.

Gregory D, Rowntree PR. 1990. A mass-flux convection scheme with representation of cloud ensemble characteristics and stability dependence closure. *Mon. Weather Rev.* **118**: 1483–1506.

Hendon HH, Wheeler MC. 2008. Some space–time spectral analyses of tropical convection and planetary-scale waves. *J. Atmos. Sci.* **65**: 2936–2948. https://doi.org/10.1175/2008JAS2675.1.

Houze RA Jr. 1989. Observed structure of mesoscale convective systems and implications for large-scale heating. *Q. J. R. Meteorol. Soc.* **115**: 425–461.

Houze RA Jr. 1997. Stratiform precipitation in regions of convection: A meteorological paradox? *Bull. Am. Meteorol. Soc.* **78**: 2179–2196.

Illingworth A, Thompson R. 2011. 'Radar bright band correction using the linear depolarisation ratio'. In *Weather Radar and Hydrology*, Proceedings of a Symposium held in Exeter, UK, April 2011. IAHS Publication 3XX, 2011.

Johnson RH, Ciesielski PE, Hart KA. 1996. Tropical inversions near the 0°C level. *J. Atmos. Sci.* **53**: 1838–1855.

Johnson RH, Rickenbach TM, Rutledge SA, Ciesielski PE, Schubert WH. 1999. Trimodal characteristics of tropical convection. *J. Climate* **12**: 2397–2418.

Jourdain NC, Sen Gupta A, Taschetto AS, Ummenhofer C, Moise AF, Ashok K. 2013. The Indo-Australian monsoon and its relationship to ENSO and IOD in reanalysis data and CMIP3/CMIP5 simulations. *Clim. Dyn.* **41**: 3073–3102.

Keenan T, May P, Holland G, Rutledge S, Carbone R, Wilson J, Moncrieff M, Crook A, Takahashi T, Tapper N, Platt M, Hacker J, Sekelsky S, Saito K, Gage K. 2000. The Maritime Continent Thunderstorm Experiment (MCTEX): Overview and some results. *Bull. Am. Meteorol. Soc.* **81**: 2433–2455.

Klingaman NP, Woolnough SJ. 2014. Using a case-study approach to improve the Madden–Julian oscillation in the Hadley Centre model. *Q. J. R. Meteorol. Soc.* **140**: 2491–2505. https://doi.org/10.1002/qj.2304.

Lin J, Mapes B, Zhang M, Newman M. 2004. Stratiform precipitation, vertical heating profiles, and the Madden–Julian Oscillation. *J. Atmos. Sci.* **61**: 296–309.

Lock AP, Brown AR, Bush MR, Martin GM, Smith RNB. 2000. A new boundary layer mixing scheme. Part I: Scheme description and single column model tests. *Mon. Weather Rev.* **128**: 3187–3199.

Mapes BE, Zuidema P. 1996. Radiative-dynamical consequences of dry tongues in the tropical atmosphere. *J. Atmos. Sci.* **53**: 620–638.

Neale RB, Slingo JM. 2003. The maritime continent and its role in the global climate: A GCM study. *J. Climate* **16**: 834–848.

Sahany S, Neelin JD, Hales K, Neale RB. 2012. Temperature–moisture dependence of the deep convective transition as a constraint on entrainment in climate models. *J. Atmos. Sci.* **69**: 1340–1358.

Schiro KA, Neelin JD, Adams DK, Lintner BR. 2016. Deep convection and column water vapor over tropical land versus tropical ocean: A comparison between the Amazon and the tropical western Pacific. *J. Atmos Sci.* **73**: 4043–4063.

Schumacher C, Houze RA Jr, Kraucunas I. 2004. The tropical dynamical response to latent heating estimates derived from the TRMM precipitation radar. *J. Atmos. Sci.* **61**: 1341–1358.

Sobel AH, Bretherton CS. 2000. Modelling tropical precipitation in a single column. *J. Climate* **13**: 4378–4392.

Sud YC, Walker GK. 2003. Influence of ice-phase physics of hydrometeors on moist-convection. *Geophys. Res. Lett.* **30**: 1758. https://doi.org/10.1029/2003GL017587.

Walters DNM, Best J, Bushell AC, Copsey D, Edwards JM, Falloon PD, Harris CM, Lock AP, Manners JC, Morcrette CJ, Roberts MJ, Stratton RA, Webster S, Wilkinson JM, Willett MR, Boutle IA, Earnshaw PD, Hill PG, MacLachlan C, Martin GM, Moufouma-Okia W, Palmer MD, Petch JC, Rooney GG, Scaife AA, Williams KD. 2011. The Met Office Unified Model Global Atmosphere 3.0/3.1 and JULES global land 3.0/3.1 configurations. *Geosci. Model Dev.* **4**: 919–941.

Wheeler M, Kiladis G. 1999. Convectively coupled equatorial waves: Analysis of clouds and temperature in the wavenumber– frequency domain. *J. Atmos. Sci.* **56**: 374–399.

Walters D, Boutle I, Brooks M, Melvin T, Stratton R, Vosper S, Wells H, Williams K, Wood N, Allen T, Bushell A, Copsey D, Earnshaw P, Edwards J, Gross M, Hardiman S, Harris C, Heming J, Klingaman N, Levine R, Manners J, Martin G, Milton S, Mittermaier M, Morcrette C, Riddick T, Roberts M, Sanchez C, Selwood P, Stirling A, Smith C, Suri D, Tennant W, Vidale PL, Wilkinson J, Willett M, Woolnough S, Xavier P. 2017. The Met Office Unified Model Global Atmosphere 6.0/6.1 and JULES Global Land 6.0/6.1 configurations, *Geosci. Model Dev*. **10**: 1487–1520, https://doi.org/10.5194/gmd-10-1487-2017.

Walters D, Baran A, Boutle I, Brooks M, Edwards J, Furtado K, Hill P, Lock A, Manners J, Morcrette C, Mulcahy J, Sanchez C, Smith C, Stratton R, Tennant W, Tomassini L, Van Weverberg K, Vosper S, Browse J, Bushell A, Dalvi M, Earnshaw P, Essery R, Gedney N, Hardiman S, Johnson B, Johnson C, Jones A, Mann G, Milton S, Rumbold H, Sellar A, Ujiie M, Whitall M, Williams K, Zerroukat M, "*HYPERLINK*"*/trac/GA/raw-attachment/wiki/GApapers/GADP/GA7.0/GA7p0.pdf*"*The Met Office Unified Model Global Atmosphere 7.0/7.1 and JULES Global Land 7.0 configurations*", to be submitted to Geosci. Model Dev., in preparation.

Wilson DR, Bushell AC, Kerr-Munslow AM, Price JD, Morcrette CJ. 2008. A prognostic cloud fraction and condensation scheme. I: Scheme description. *Q. J. R. Meteorol. Soc*. **134**: 2093–2107.

Wolding BO, Maloney ED. 2015. Objective diagnostics and the Madden–Julian Oscillation. Part II: Application to moist static energy and moisture budgets. *J. Climate* **28**: 7786–7808. https://doi.org/10.1175/JCLI-D-14-00689.1.

Yokoi S. 2015. Multi-reanalysis comparison of variability in column water vapour and its analysis increment associated with the Madden–Julian oscillation. *J. Climate* **28**: 793–808. https://doi.org/10.1175/JCLI-D-14-00465.1.

Zhu H, Hendon HH. 2015. Role of large-scale moisture advection for simulation of the MJO with increased entrainment. *Q. J. R. Meteorol. Soc.* **141**: 2127–2136.

Zhu H, Sobel AH. 2012. Comparison of a single-column model in weak temperature gradient mode to its parent AGCM. *Q. J. R. Meteorol. Soc.* **138**: 1025–1034. https://doi.org/10.1002/qj.967.

